SAR Simulation Report
Version 1.0.1

Model No.	FCC ID
A2580 (1 meter)	BCGA2580
A3250 (2 meter)	BCGA3250

Date of Simulation:
05/01/2024-07/15/2024
Location:
Apple Inc., Cupertino, CA, USA

Revision history

Revision	Date	Description
1.0.1	24 July, 2024	Initial Release of SAR Simulation API tool report

Table of Contents

List of Figures:

List of Tables:

1 Introduction

This report demonstrates RF exposure compliance using SAR simulation for 2024 Apple MagSafe model (FCC IDs: BCGA2580, BCGA3250) operating at 360 kHz. Apple uses this frequency in addition to 127.7 kHz.

To demonstrate RF exposure compliance at 360 kHz and 127.7 kHz operating frequencies, as permitted by §2.1093 (certification for portable devices below 4 MHz), SAR numerical simulations are performed to demonstrate compliance to the 1.6 W/Kg localized 1-g SAR limit.

The following sections describe the modeling, measured H-field, simulated H-field, and simulated SAR.

2 Wireless Power Transfer System

The wireless power transfer system consists of a transmitting coil with 11 turns and measures 7.26 uH nominally in free air. The receiver coil consists of 13 turns and measures 9.47 uH nominally in free air. Both coils are wound spirally and made of stranded wire, details about the coils are listed below.

Tx Coil Winding Type	Spiral, 1 Layer, Stranded Wire
Turns	11
Inner Radius	11.14 mm
Outer Radius	18.37mm
Cross-section	Rectangular
Thickness	1 mm
Width	0.5 mm

Rx Coil Winding Type	Spiral, 1 Layer, Stranded Wire
Turns	13
Inner Radius	10.18 mm
Outer Radius	20.94 mm
Cross-section	Rectangular
Thickness	0.13 mm
Width	0.68 mm

Below, are key parameters of the design that will be helpful in determining worst-case use for exposure:

Table 1. Key design parameters

Receiver	**Phone**	**Phone**	**AirPod**
Max Power Delivered to Tx Coil	Up to 33.4 W	Up to 10 W	Up to 2.61 W
Full Charge Time	2 hours 30 minutes	5 hours	2 hours 26 minutes
Operating Frequency	f_0 = 360 kHz	f_0 = 127.7 kHz	f_0 = 127.7 kHz
Communications/Modulation Method	ASK for Phone to Charger (load modulation) FSK for Charger to Phone	ASK	ASK
Object Detection Mode	Low Power Pulse	Low Power Pulse	Low Power Pulse

3 SAR Simulations Methodology

The following steps have been taken to show the validity of the model used for the SAR simulations:

1) EM Simulation:
    a. Import a CAD model that represents the actual product in the simulation tool.
    b. Define material properties inside the product based on vendor's inputs.
    c. Extract two-port network impedance matrix ([Z]) from the simulation.
2) Circuit Simulation:
    a. Include the impedance matrix in the wireless power transfer (WPT) circuit model.
    b. Run circuit simulation and extract coils' current waveforms.
3) Field Calculations:
    a. Use the current waveforms to drive the EM simulation model.
    b. Calculate H-field from the simulation.
4) Validate Simulation Model:
    a. Measure H-field, and compare with simulation result.
    b. Perform full uncertainty analysis.
    c. Once a correlation is established and model's accuracy is verified, this model will be used for computational exposure assessments (e.g., SAR simulations).

The entire workflow is summarized and shown in Fig. 1.

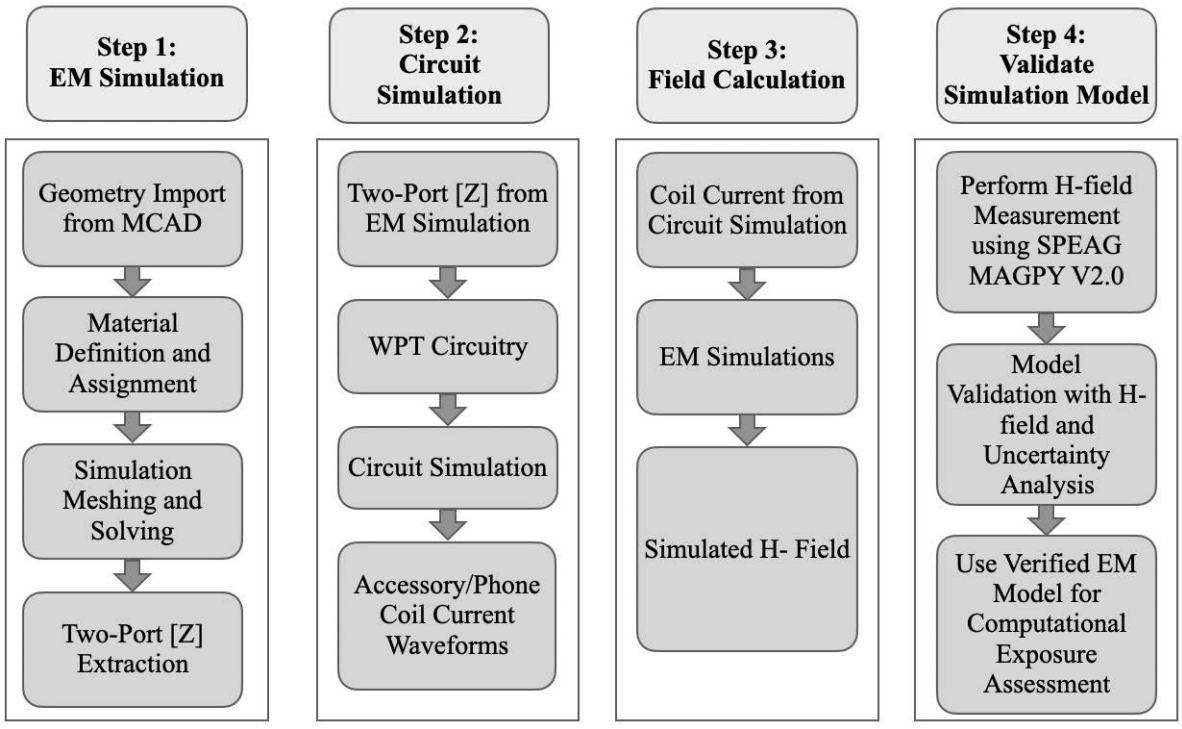

Figure 1: Model validation workflow for computational exposure assessment.

4 H-field Simulations for Transmitter

The Electromagnetics simulations are conducted using commercially available software ANSYS HFSS. To validate the simulation model, H-field measurements are made on the DUT and compared to the simulated model results. The validated model is then used for SAR simulations.

SPEAG Magnetic Amplitude and Gradient Probe System (MAGPY) V2.0 shown in Fig. 2 is used to measure the H-field. This probe consists of 24 small loop sensors arranged on the corners of a 22mm cube used for measuring H-field amplitude and gradient. The lower measuring loops are 7.5mm from the probe tip enabling a closer measurement to the electromagnetic source. Probe specifications are described in Table 2.

Figure 2: SPEAG MAGPY V2.0 measurement probe.

Table 2. Probe Specifications:

Model	MAGPY V2.0
Frequency	3 kHz – 10 MHz
Measurement Center	18.5 mm from the probe tip
Dimensions: (H-field sensor loop size) (E-field sensor arm length) (Overall Diameter)	1 cm^2 50 mm 60 mm
Dynamic Range	0.08 to 2000 V/m for Electric field 0.1 to 3200 A/m for Magnetic field
Measurement Uncertainty (Extended *k=2*)	1.3 dB
Application	Electric and Magnetic field measurement

For the simulation-measurement correlation study, a case where only the puck (Tx) is present is chosen. The measurement setup is shown in Fig. 3. As shown in the measurement setup, the center of the probe coils is 18.5 mm away from the true 0 mm touch position and lower four sensor are

7.5mm away. Following procedure was used to compute the averaged fields from the simulation results for correlating with the measured data: The volumetric H-field is exported from HFSS and post-processed using a MATLAB script to include the SPEAG MAGPY V2.0 probe averaging effect. The SPEAG MAGPY V2.0 probe has 8x3 internal loops. These loops measure H-field by integrating it over their effective aperture area. The script will apply this integration over the exported volumetric H-field. Worth mentioning that the script does not consider any potential loading effect that the probe may have on the DUT, including mutual interaction with the DUT coils. To our experience, this mutual interaction is partially responsible for the discrepancy between the simulation and measurement results when the probe is touching the DUT. Detailed description of the post-processing is also shown in Fig. 4.

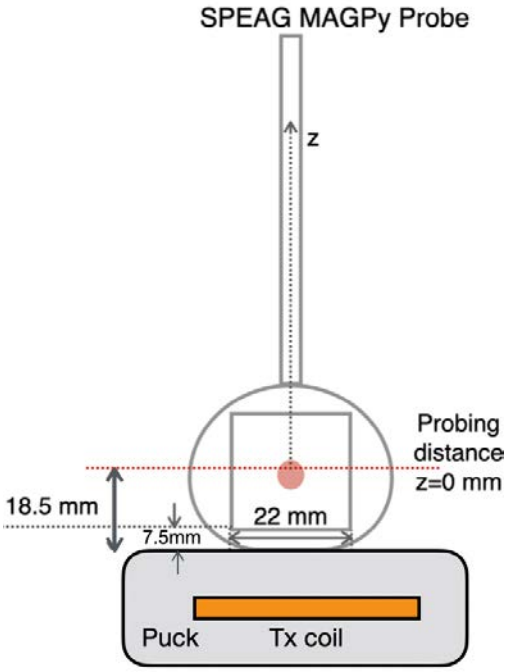

Figure 3: H-field measurement setup for direct exposure case.

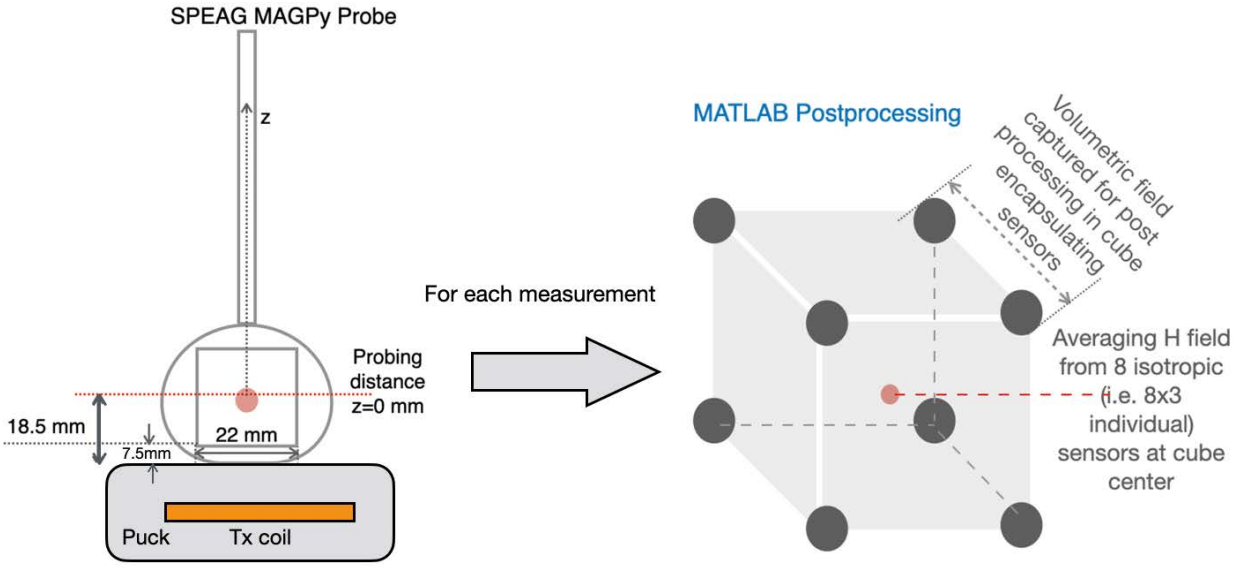

Figure 4: Post-processing using MATLAB script: Volumetric field data is exported from HFSS and processed to include SPEAG MAGPY V2.0 probe effect.

The correlation between the simulations and measurements are performed at a vertical distance away from the DUT while the probe is moved vertically in Z direction from 0 mm (probe center) with the step size of 2 mm till 25 measurements are taken. The results are shown in Fig. 5.

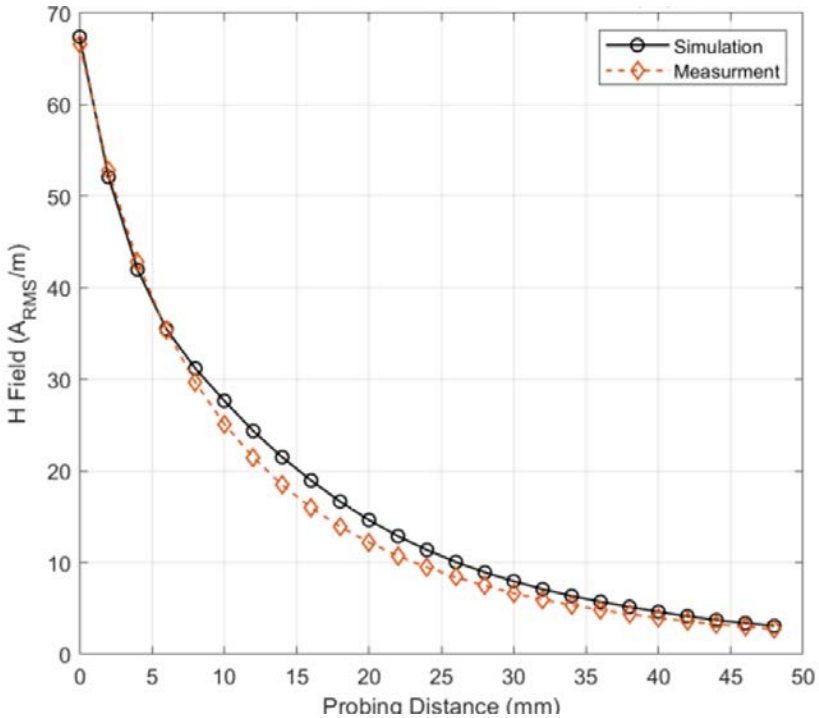

Figure 5: Probe moving away from puck: simulated vs measured H-field comparison.

Based on the provided graphs in Fig. 5 there is a good correlation between the measurements and simulations. This validated simulation model is then used for the SAR simulations in the next sections.

5 SAR Simulations

The validated simulation model is used for SAR calculations with a phantom added in contact with the DUT. The simulations are computed on a 96 core CPU server with an available RAM of 4 Terabytes. For this simulation, the model run takes approximately 6 hours to complete.

The following steps are used for accurate SAR calculations:

1) Elliptical phantom used in body exposure measurements is commercially available from SPEAG: Outer Dimensions of 600mm x 400mm x 150mm.
2) Homogeneous tissue material is used as liquid for desired frequency.
3) Power loss in phantom is calculated.
4) Divide power loss by mass density to calculate SAR.

$$SAR = \frac{P_l}{\rho}$$

$$P_l = \text{Power loss density}$$

$$\rho = \text{Mass density}$$

5) Point SAR is averaged over 1g or 10g tissue.
6) For SAR simulations, mass density of 1000 Kg/m^3 is used for the Phantom.

Human Tissue Material Properties:
The worst-case scenario has been identified to be when a user is holding the device in hand and taking a call or holding the phone on their body while charging. Since the SAR phantom is homogenous, using the layers' properties [3-7], for the SAR simulations the phantom with conductivity of 0.75 S/m and permittivity of 55 is used.

Mesh Adaptation:
HFSS adapts the mesh based on field strength. It is important to ensure the mesh is refined to capture SAR accurately. This can be done by using adaptive meshing available in HFSS and mesh refinement process described in Fig. 6.

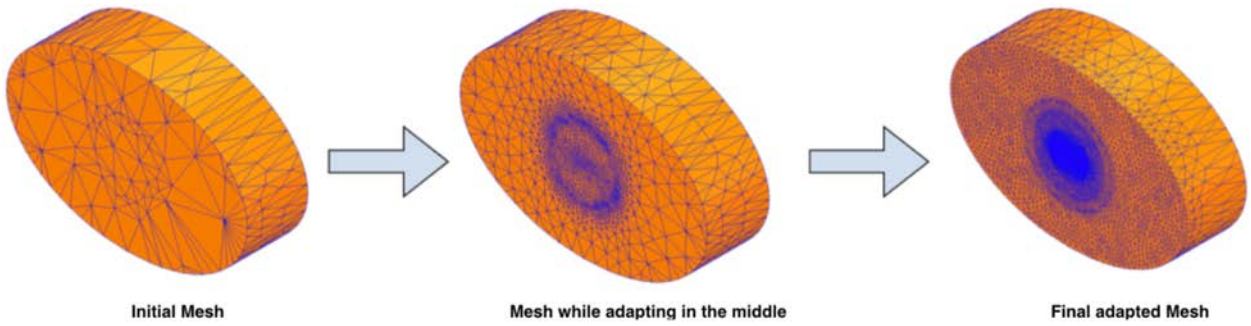

Figure 6: Initial mesh generation and refinement through adaptive meshing technique in HFSS.

SAR Results:

Using the H-field simulation and measurement tables, two exposure cases were selected for SAR investigation. Considering that the phantom can be in contact with the phone or puck, there is a total of four scenarios.

5.1 Exposure Cases:

Exposure Case 000 (a): Nominal configuration with perfect alignment and phantom placed above the phone.
Exposure Case 000 (b): Nominal configuration with perfect alignment and phantom placed below the puck.
Exposure Case 404 (a): Misaligned configuration and phantom placed above the phone.
Exposure Case 404 (b): Misaligned configuration and phantom placed below the puck.

For the simulations, the coil properties are also fixed, transmitting coil with 11 turns and measures 7.26 uH nominally in free air. The receiver coil consists of 13 turns and measures 9.47 uH nominally in free air. Both coils are wound spirally.

The following outputs are calculated and reported in the Table:

a. Peak spatial 1-g average SAR in tissue.
b. Peak spatially averaged electric field in tissue. Electric field is spatially averaged in a contiguous tissue volume of 2 mm by 2 mm by 2 mm.

The simulation results for the selected use cases at 360 kHz are listed in the Table 3, below.

Table 3: Averaged 1-g SAR and Peak Spatial Average E-field (inside Phantom) simulation results at 360 kHz for the nominal use cases

	Orientation	Description	Peak Spatial Average SAR (W/Kg) Averaged over 1 gram	Peak Spatial Average E-field (V/m) Averaged over 2x2x2 mm^3
Optimal Placement (Max Coupling)	Phone side	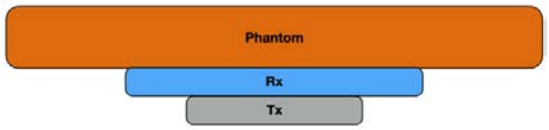	0.00000012	0.03
	Puck side		0.0000017	0.12
Offset Δx=4mm, Δz=4mm	Phone side	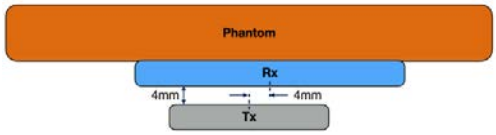	0.0000015	0.12
	Puck side	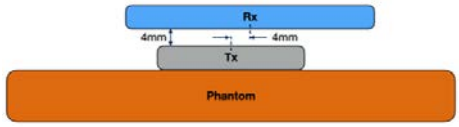	0.000017	0.32

SAR plot is shown in Fig. 7 (a) for Case404(b). The peak spatial 1-g average SAR is 0.000017 W/kg. The side view is also presented as shown in Fig. 7 (b) below.

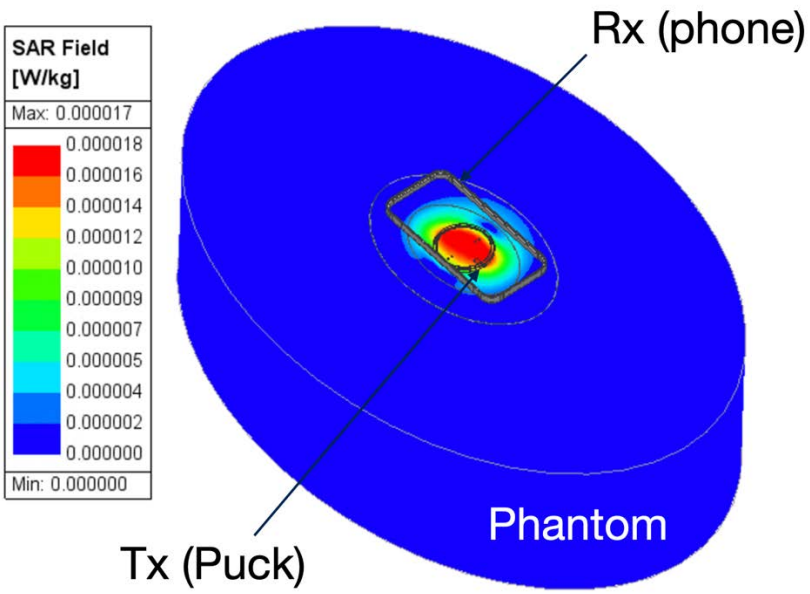

(a) Full view of average SAR plot for Case 404 (b)

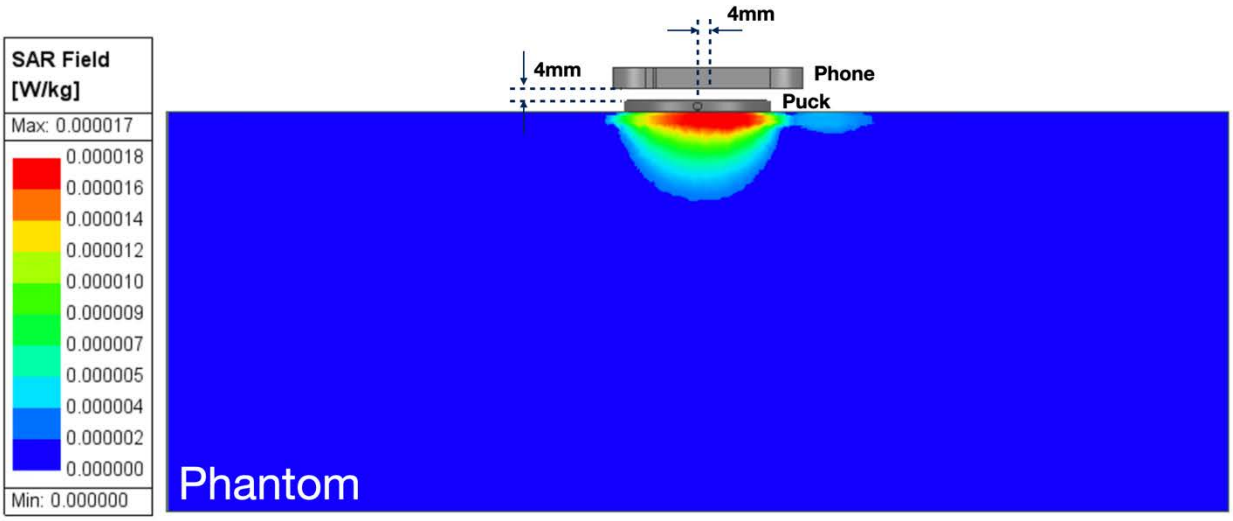

(b) Side view of average SAR plot for Case 404 (b)

Figure 7: Spatial 1-gram average SAR for Case 404 (b), (a) full view, (b) side view.

5.2 Additional Exposure Cases

In addition, a corner case was also investigated that is not likely to happen in normal application when the puck (Tx) is in direct contact with the phantom with no phone present.
Peak 1-g averaged SAR and E-field inside the phantom for the Direct Exposure case is shown below. For this direct exposure case study, we are also including 127.7 kHz frequency that is used for AirPod and phone charging.

Direct Exposure (unrealistic) Case 1: with receiver absent and the phantom facing towards the puck (Tx) coil at 360 kHz.
Direct Exposure (unrealistic) Cases 2 & 3: with receiver absent and the phantom facing towards the puck (Tx) coil at 127.7 kHz for (one case for Aipod and one for Phone).

Table 4. Averaged 1-g SAR and peak spatial average E-field (inside Phantom) simulation results for direct exposure.

Exposure Case	Description	Peak Spatial Average SAR (W/Kg) Averaged over 1 gram	Peak Spatial Average E-field (V/m) Averaged over 2x2x2 mm^3
Case 1 360 kHz	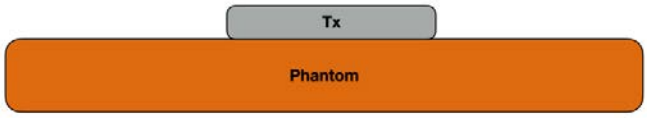	0.125	43.62
Case 2 127.7 kHz (Phone)	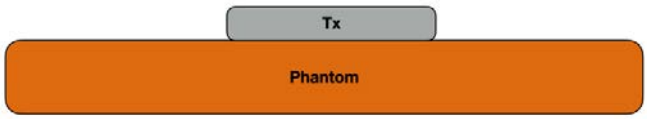	0.0249	19.66
Case 3 127.7 kHz (AirPod)	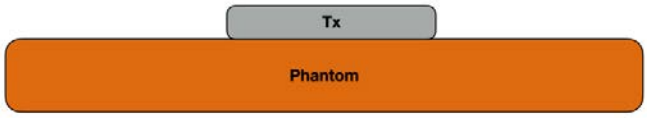	0.008	11.23

SAR plot is shown in Fig. 8 for Direct Exposure Case 1.

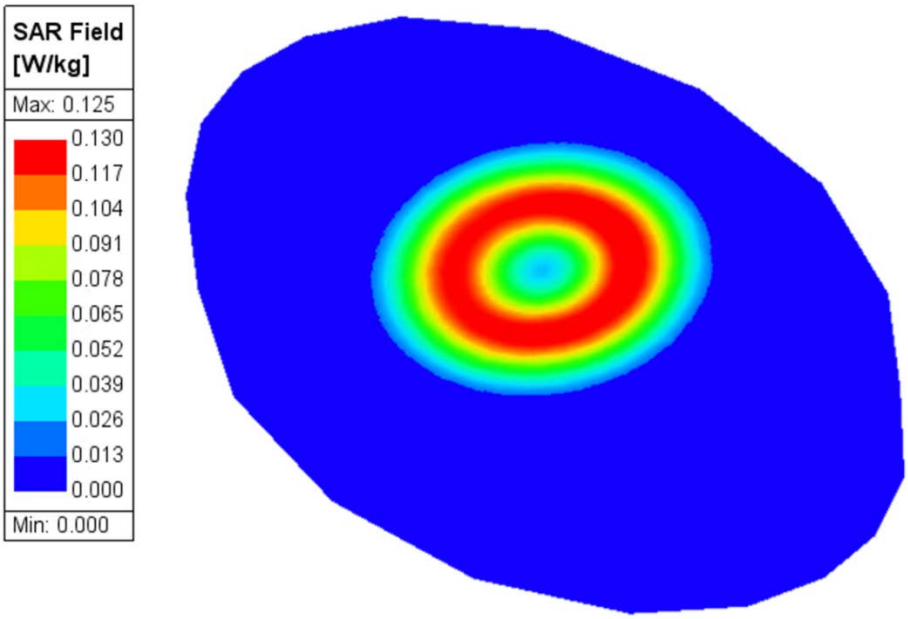

(a) Average SAR plot for Direct Exposure Case 1.

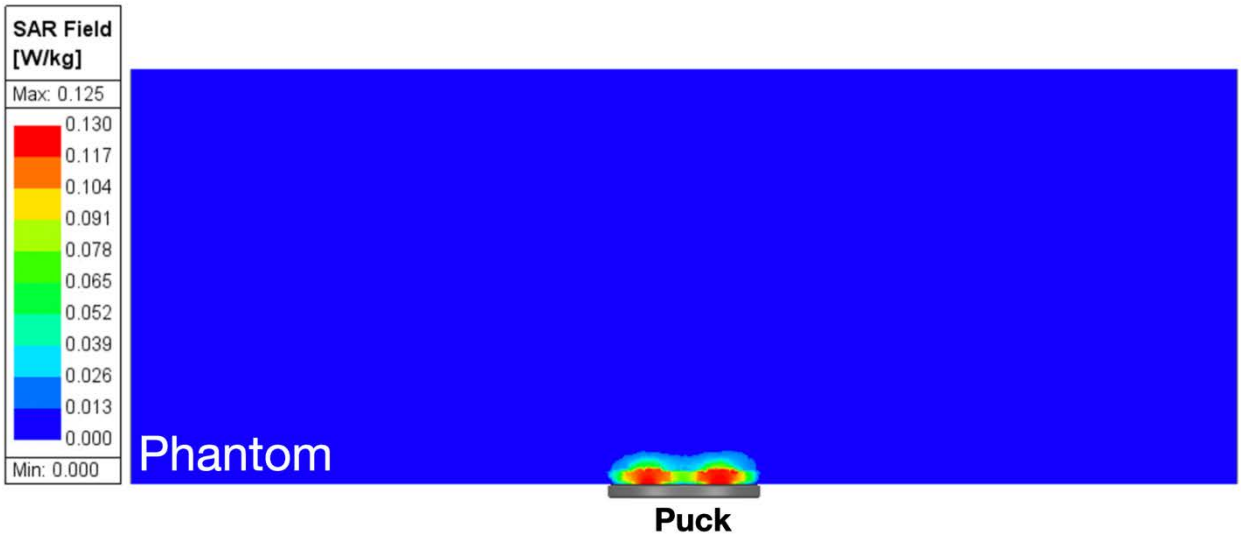

(b) Side view of average SAR plot for Direct Exposure Case 1.

Figure 8: Spatial 1-gram average SAR for Direct Exposure Case 1, (a) full view, (b) side view

E-field distribution inside the phantom for the Case1(a) is shown below. Please note that the value reported in the table above was averaged over a cube of 2mmx2mmx2mm and that explains why the value is lower than the peak E-field in this plot.

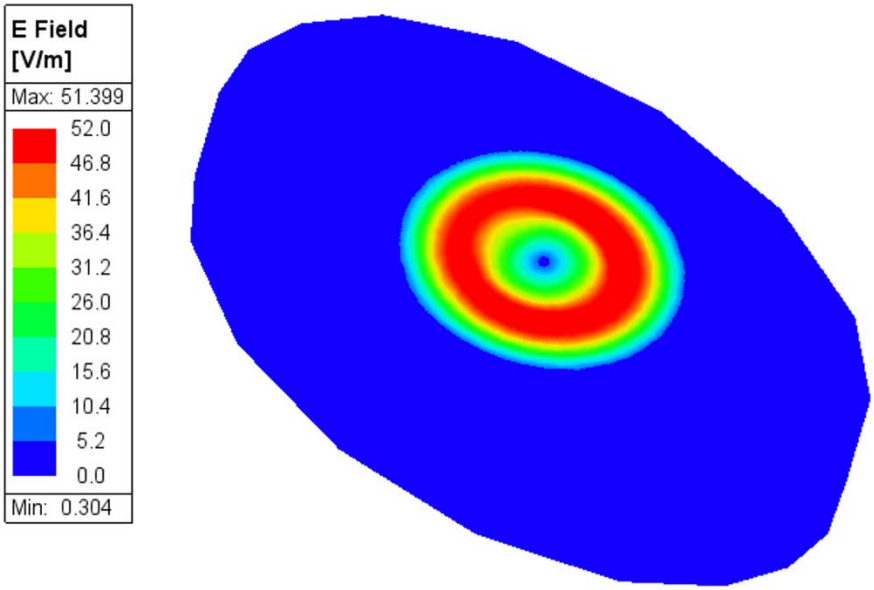

Figure 9: Peak E-field distribution inside Phantom for Direct Exposure Case 1.

As another case, SAR plot is shown in Fig. 10 for Direct Exposure Case 3.

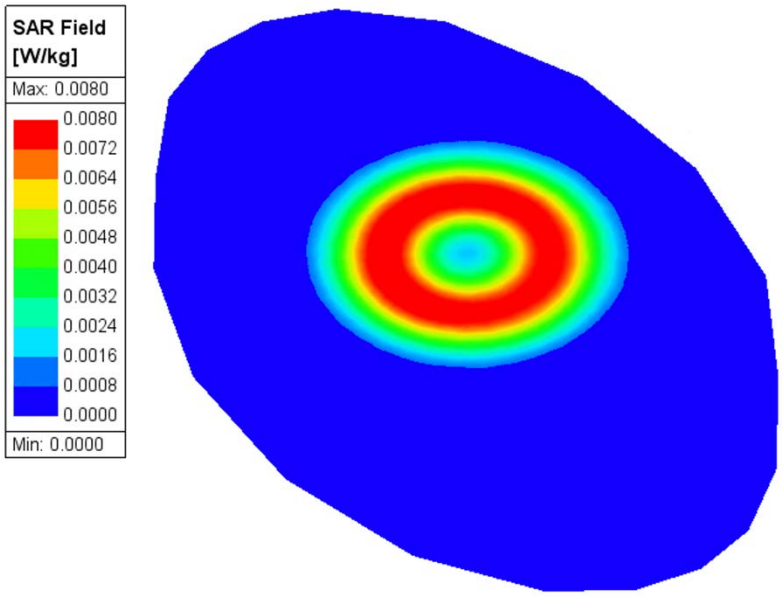

(a) Average SAR plot for Direct Exposure Case 3.

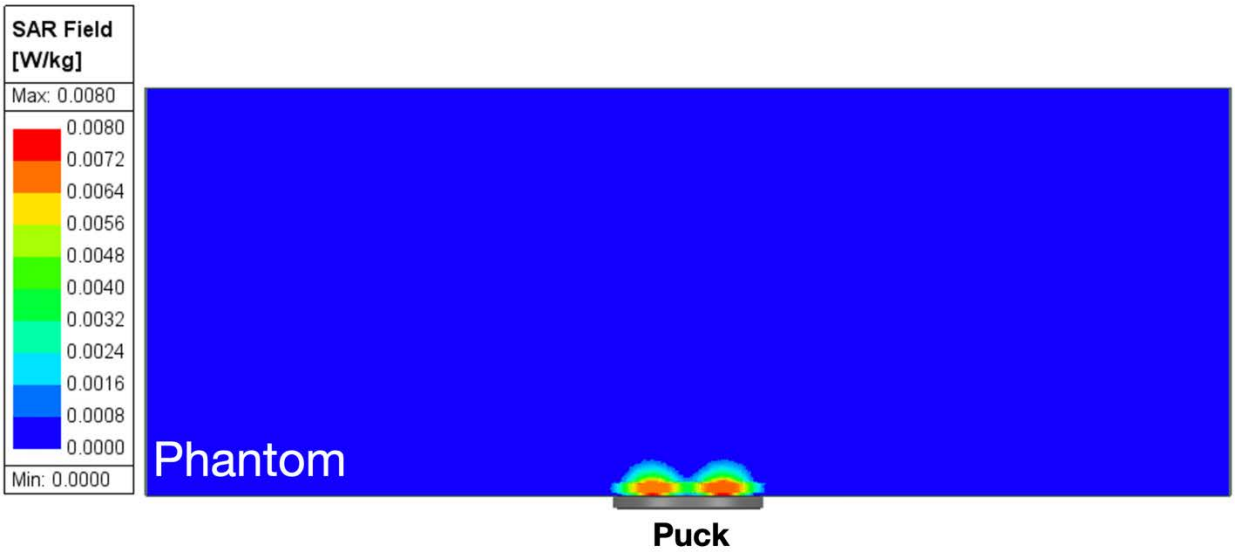

(a) Side view of average SAR plot for Direct Exposure Case 3.

Figure 10: Spatial 1-gram average SAR for Direct Exposure Case 2, (a) full view, (b) side view

E-field distribution inside the phantom for the Case 3 is shown, below. Please note that the value reported in the table above was averaged over a cube of 2mmx2mmx2mm and that explains why the value is lower than the peak E-field in this plot.

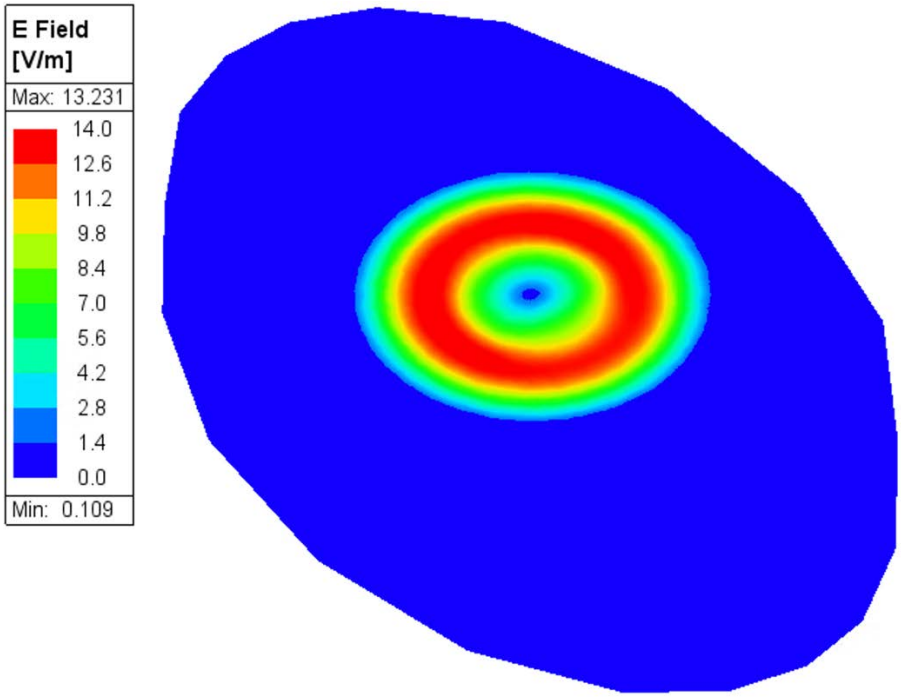

Figure 11: Peak E-field distribution inside phantom for Direct Exposure Case 3.

Summary

Based upon the above results, the accuracy of the SAR simulations is demonstrated by correlating H-field measurements to simulations. The validity of using this modeling and SAR computational method hence is established for wireless charger models FCC IDs: BCGA2580, BCGA3250. Among the exposure cases, the highest peak spatial 1-gram averaged SAR of 0.000017 W/Kg and the highest peak spatial average E-field (i.e., averaged over a cube of 2 mm x 2 mm x 2 mm) of 0.32 V/m, is observed when the puck and the phone are misaligned.

Overall, the SAR is significantly lower than the SAR limit of 1.6 W/Kg (below 0.01% of the actual SAR limit). Therefore, we respectfully request that the allowance to use of this model to demonstrate RF Exposure compliance for Apple's proposed WPT products.

Annex: Specific Information for SAR Computational Modelling

1) Computation Resources

The models were simulated on a 96 core CPU server with an available RAM of 4 Terabytes. Each model variation took around 6 hours to complete. Based on the simulation profile, the minimum resources needed to finish these simulations will be approximately 8 core CPU with 512 GB of RAM. Using the minimum requirements simulation will likely take more time than 10 hours.

2) Algorithm implementing and validation

This section is divided into two parts. The code performance validation provides methods to determine that the finite-element algorithm in HFSS has been implemented correctly and works accurately within the constraints due to the finite numerical accuracy. It further determines the quality of absorbing boundary conditions and certain parts of the post processing algorithms that are part of HFSS. The second part has few canonical benchmarks. All benchmarks can be compared to analytical solutions of the physical problem or its numerical representation. The methods characterize the implementation of the finite-element algorithm used by HFSS in a very general way. They are defined such that it is not possible to tune the implementation for a particular benchmark or application without improving the overall quality of the code.

2.1) Code performance validation

2.1.1) Propagation homogeneous medium

A straight rectangular waveguide with ports on both ends is well suited as a first test of an implementation of the Finite-Element Method used by HFSS. The waveguide has a width of 20 mm, a height of 10 mm and a length of 300 mm. The waveguide is filled homogeneously with a material which, in three separate simulations, shall assume the following properties:

i. $\varepsilon r = 1$, $\sigma = 0$ S/m;
ii. $\varepsilon r = 2$, $\sigma = 0$ S/m;
iii. $Re(\varepsilon r) = 2$, $\sigma = 0.2$ S/m.

To verify that the mesh used by HFSS is independent of orientation, the waveguide has been rotated so that it is not parallel with any principal coordinate plane (XY, XZ, YZ). The waveguide is driven in the TE10 mode at 10 GHz. Reported are the magnitudes of S21 and S11, as well as the values of the real and imaginary parts of the propagation constant γ. The table 5, below provides the reference values [B1], acceptable result criteria, as well as the simulated results.

Table 5: Criteria for the waveguide evaluation

$Re(\varepsilon_r)$	1	2	2
σ	0	0	0.2
|S21| reference value	1	1	8.7 × 10-5
Criterion for |S21|	≥ 0.9999	≥ 0.9999	± 5 × 10-6
|S21| simulated results	1	1	8.7 × 10-5
|S11| reference value	0	0	0
Criterion for |S11|	≤ 0.003	≤ 0.003	≤ 0.003
|S11| simulated results	0	0	0
$Re(\gamma)$ reference value	0	0	31.17 m-1
Criterion for $Re(\gamma)$	± 0.1 m-1	± 0.1 m-1	± 2%
$Re(\gamma)$ simulated results	0	0	31.17
$Im(\gamma)$ reference value	138.75 m-1	251.35 m-1	253.28 m-1
Criterion for $Im(\gamma)$	± 2%	± 2%	± 2%
$Im(\gamma)$ simulated results	138.75	251.35	253.28

As is seen in the above table, HFSS easily meets the criteria for properly and accurately calculating the waveguide problem.

2.1.2) Planar dielectric boundary

In order to test the reflection of a plane wave by a dielectric boundary, a rectangular waveguide can again be used. It is well known that the TE10 mode can be thought of as a superposition of two plane waves [1]. Each wave's direction of propagation makes an angle θ with the axis of the wave guide, given by

$$\cos^2\theta = 1 - (c/2af)^2 \quad (1)$$

where c is the speed of light, a is the width of the wave guide and f is the frequency. Assuming the axis of the waveguide is the Z axis and assuming the waveguide is filled with vacuum for Z>0 and filled with dielectric 1 with complex relative permittivity εr for Z<0, Fresnel reflection coefficients for the TE and the TM cases, defined as ratios of electric field strengths, are given by [2]

$$R^{TE} = (k_{0,z} - k_{1,z}) / (k_{0,z} + k_{1,z}) \quad (2)$$

$$R^{TM} = (\varepsilon_r k_{0,z} - k_{1,z}) / (\varepsilon_r k_{0,z} + k_{1,z}) \quad (3)$$

where $k_{0,z}$ and $k_{1,z}$ denote the z component of the propagation vector of the plane wave in vacuum and in the dielectric, respectively. They can be evaluated through

$$k_{0,z} = k_0 \cos\theta \quad (4)$$
$$k_{1,z} = k_0 \sqrt{(\varepsilon_r - \sin^2\theta)} \quad (5)$$

Finally, ε_r is complex and is given by

$$\varepsilon_r = \mathrm{Re}(\varepsilon_r) - j\sigma/(2\pi f\varepsilon_0) \quad (6)$$

where $\mathrm{Re}(\varepsilon_r)$ denotes the real part of the relative permittivity and σ is the conductivity of the medium.

For this test, a 20 mm × 10 mm waveguide with a length of 60 mm, as shown in Figure 12, was created. The top half was filled with vacuum and the bottom half with dielectric.

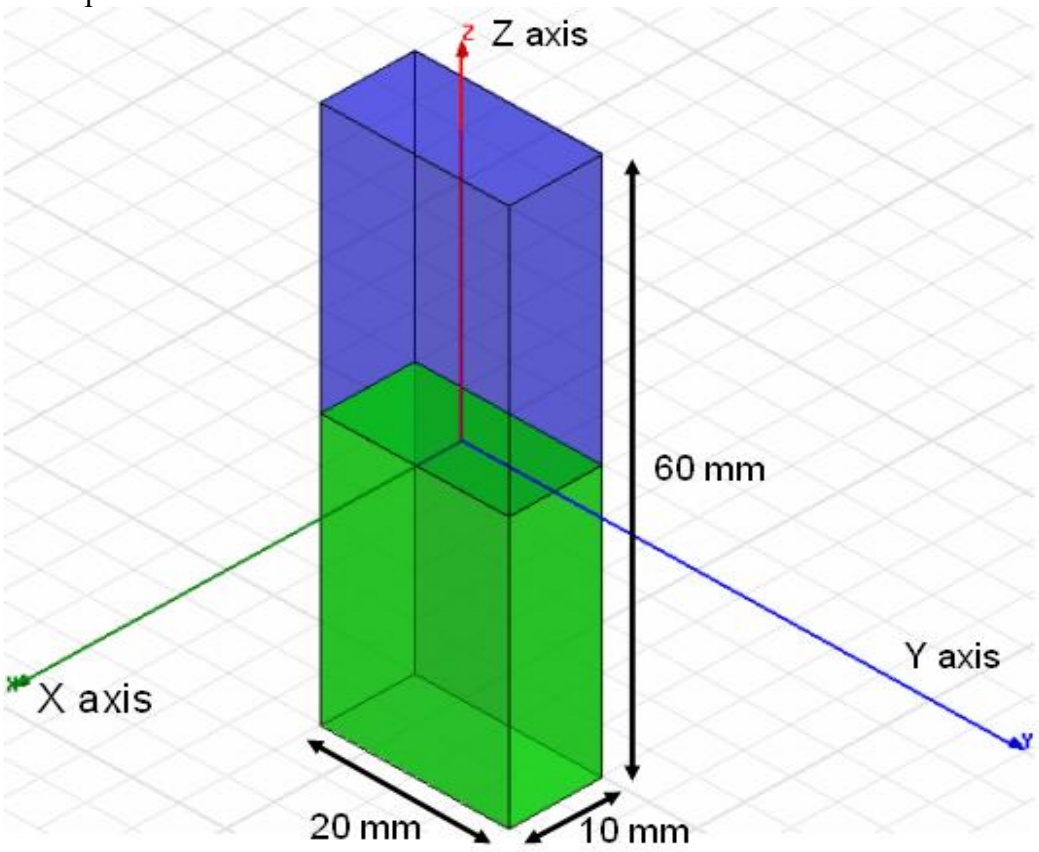

Figure 12: Waveguide filled half with vacuum and half with dielectric

In one copy of the model, all side walls were lossless metal, such that the dominant mode is the TE10 mode with propagation constant 138.75 m-1 at 10 GHz and represents the TE case in the reflection analysis. In the other copy of the model, the side walls that are parallel to the YZ plane were perfect magnetic conductors while the other walls were perfect electric conductors, such that the second mode (after a TEM mode which won't be used in this test) has propagation constant 138.75 m-1 at 10 GHz and represents the TM case in the reflection analysis.

Before simulation, the waveguides were rotated over an arbitrary angle such that no face is parallel with any coordinate plane. The waveguides were driven at 10 GHz in the proper mode. In doing so, it is good practice to calculate all propagating modes, but the coupling between modes is expected to be negligible. Simulations were run for the cases of lossless and lossy dielectric as shown in Table 6. For the HFSS to pass the test, according to IEC 62704-1, the results need to be within 2% of the analytical values given in Table 6.

Table 6: Reflection at a dielectric interface

Re(εr)	σ (S/m)	RTE	RTE- Simulated	RTM	RTM - Simulated
4	0	0.4739	0.4739	0.1763	0.1763
4	0.2	0.4755	0.4755	0.1779	0.1779
4	1	0.5105	0.5105	0.2121	0.2121

As can be seen in above table, HFSS produces results that are identical to the analytical results.

2.2) Canonical Benchmarks

The results for a few low frequency benchmarks are summarized below. These benchmarks were used to validate the accuracy of the tool at low frequencies:

2.2.1) Dipole Antenna:

The following parameter were used in the dipole antenna to resonate at 400KHz.
Dipole length: 375 meters
Feed gap: 2.5 meters
Dipole Diameter: 5 meters

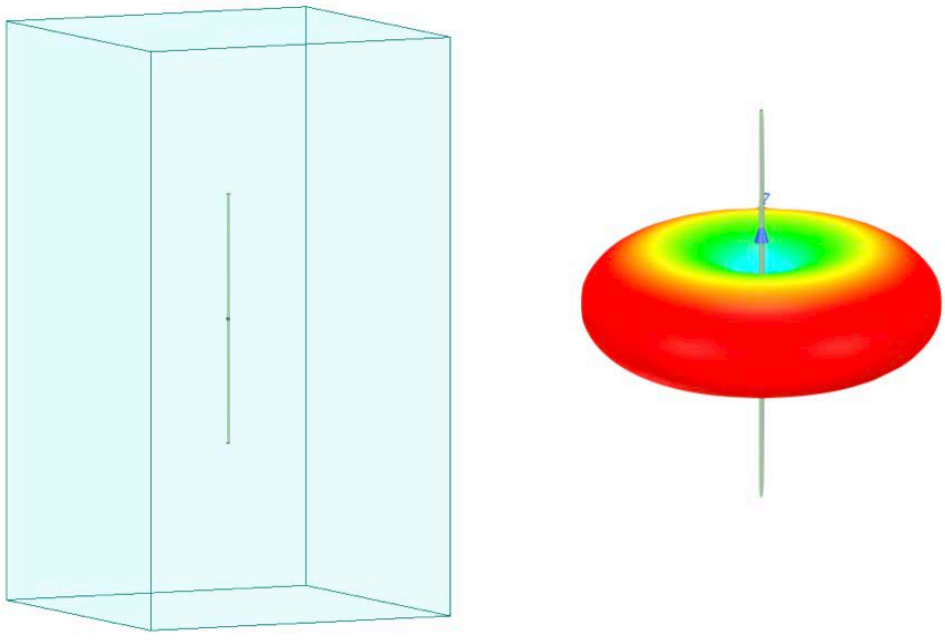

Figure 13: Dipole Antenna Model

The document IEC 62704-4 2020 was referenced to compare the tables. Two computation methods were demonstrated as shown below to show the validity of the model.

Table 7: Simulated dipole using FEM.

Quantity	Simulated Results	Tolerance	Satisfactory
Re(Z) @400 kHz	98.34 Ω		
Im(Z) @400 kHz	49.79 Ω		
Re(Z) @320 kHz	41.95 Ω	25 Ω < Re(Z) < 50 Ω	Yes
Im(Z) @320 kHz	-90.30 Ω	-50 Ω < Im(Z) < -100 Ω	Yes
Re(Z) @360 kHz	63.90 Ω	50 Ω < Re(Z) < 75 Ω	Yes
Im(Z) @360 kHz	-20.45 Ω	-25 Ω < Im(Z) < 0 Ω	Yes
Resonance Frequency Im(Z)=0	371.73 kHz	360 kHz < 380 kHz	Yes
Maximum power budget error	0.74 %	< 5 %	Yes

Table 8: Simulated dipole using MoM.

Quantity	Simulated Results	Tolerance	Satisfactory
Re(Z) @400 kHz	96.63 Ω		
Im(Z) @400 kHz	46.85 Ω		
Re(Z) @320 kHz	42.80 Ω	25 Ω < Re(Z) < 50 Ω	Yes
Im(Z) @320 kHz	-93.09 Ω	-50 Ω < Im(Z) < -100 Ω	Yes
Re(Z) @360 kHz	64.14 Ω	50 Ω < Re(Z) < 75 Ω	Yes
Im(Z) @360 kHz	-22.29 Ω	-25 Ω < Im(Z) < 0 Ω	Yes
Resonance Frequency Im(Z)=0	372.77 kHz	360 kHz < 380 kHz	Yes
Maximum power budget error	0.71	< 5 %	Yes

2.2.2) Toroid Inductor:

The parameters of the toroid were chosen to be
N = 20
A = 6.35e-4 m^2
R = 0.0263 m
ur = 64

The formula below from [9] results in an inductance of 139 uH. The model created in HFSS resulted in an inductance of 138.06 uH at 1 MHz.

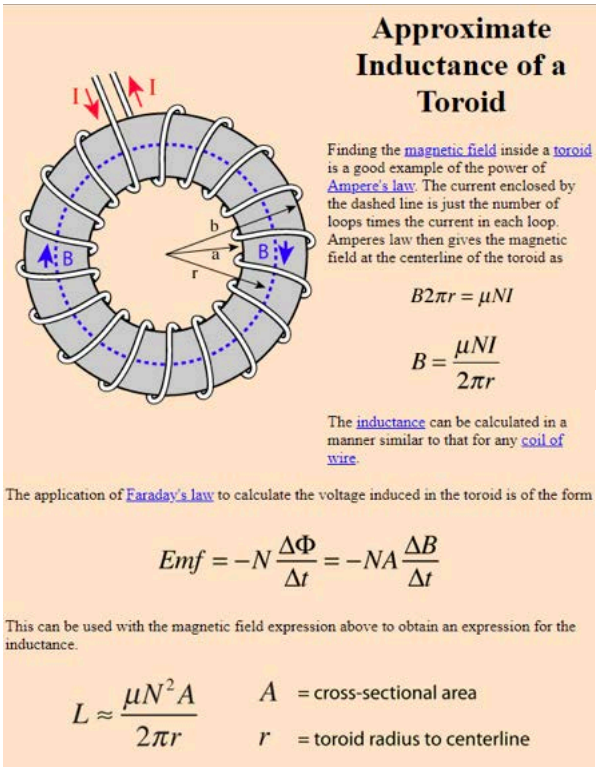

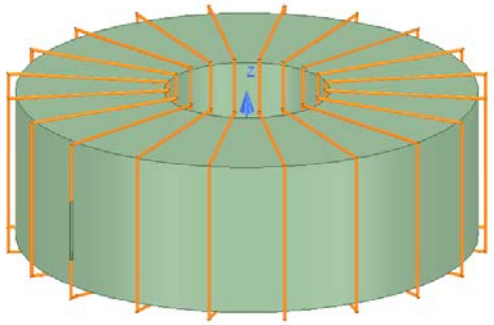

Figure 14: Toroid model.

2.2.3) Circular coil parallel to a flat, homogeneous phantom.:

The following benchmark is implemented using Equations 1-4 of the referenced Chen et al. (2014) paper. The analytical calculations using the reference resulted in 1.6 V/m, which matches the HFSS result shown in Figure 16.

Below is the coil and phantom parameters:

Coil Diameter: 50 mm
Number of Turns: 10
RMS Current: 0.707 A (Peak current = 1 A)
Frequency: 100 kHz
Coil-to-Body Distance: 5 mm
Tissue Conductivity: 0.05 S/m
Tissue Permittivity: 1120
Phantom radius: 84 mm

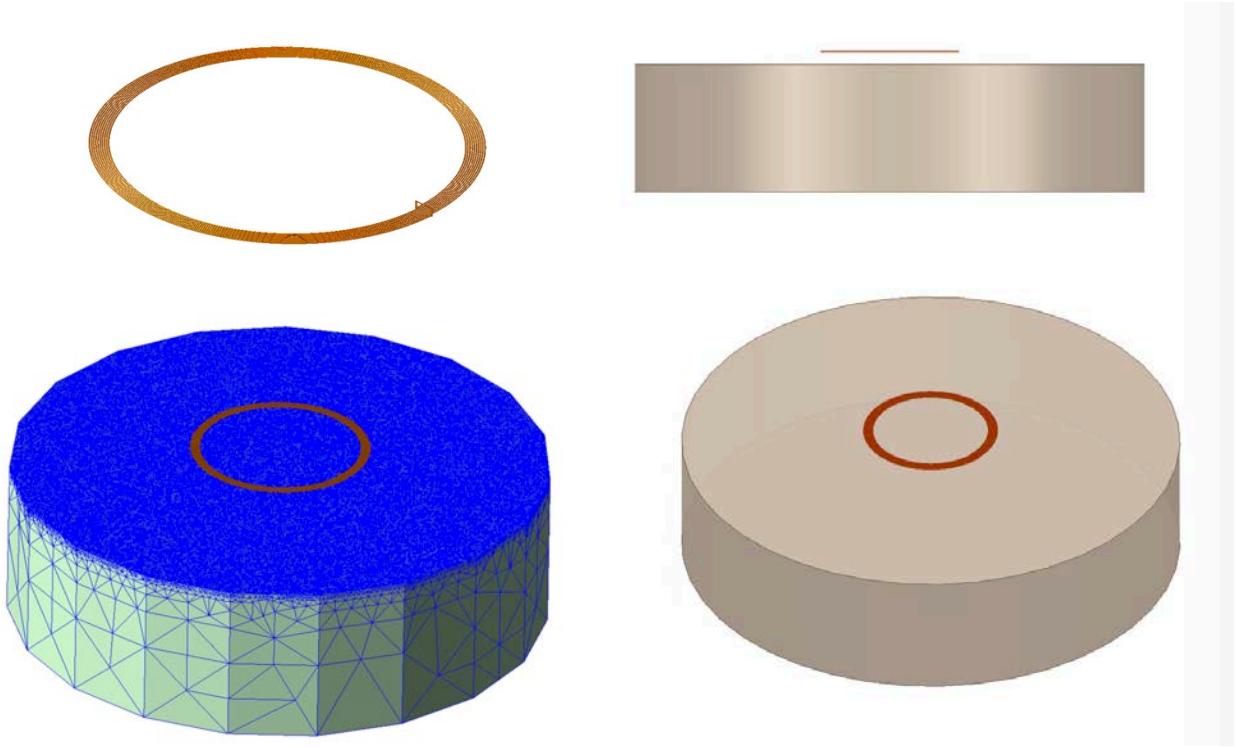

Figure 15: Current loop in front of a cuboid.

The simulated spatial peak RMS electric field in tissue is 1.55 V/m compared to the analytical value of 1.60 V/m.

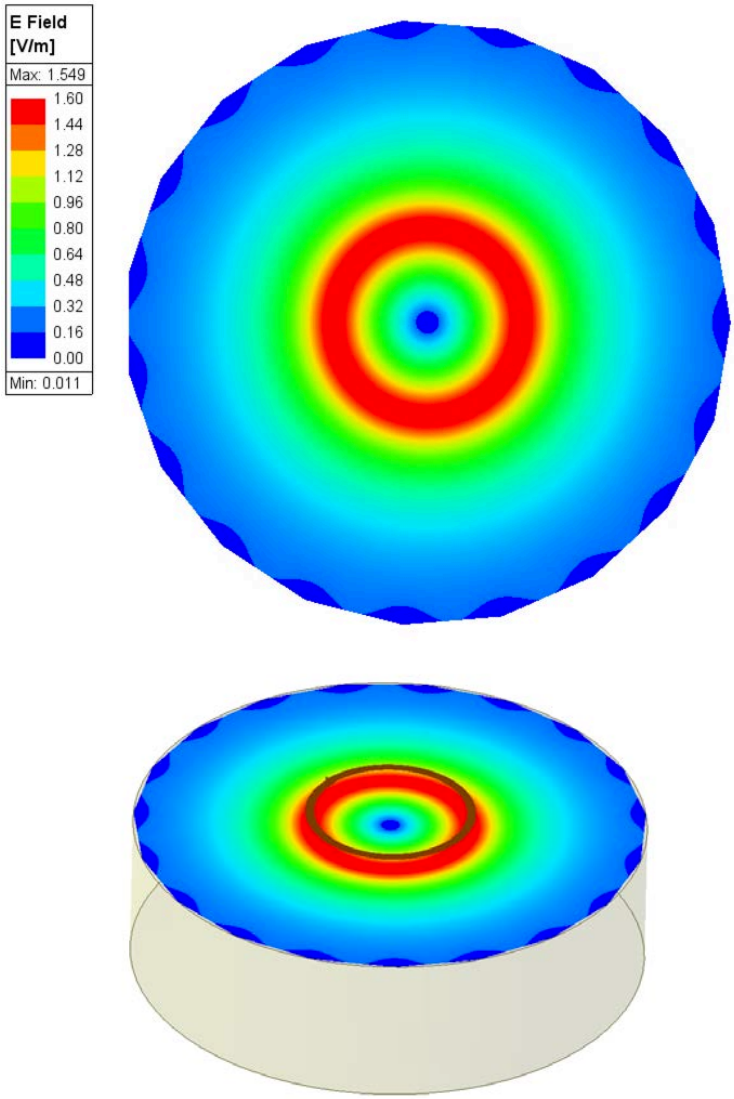

Figure 16: Electric field plots at the phantom surface.

3) Computational peak SAR from peak components & One-gram averaged SAR procedure

The calculation method for SAR follows IEEE P1528.4. Once the solver calculated the S-Parameter results, different coils can be driven and the result from the S-Parameter calculation is automatically scaled to the driving current of the coils. This result combination provides the correctly scaled power loss density in the phantom. The SAR calculation computes the local SAR first using electric field and conducting current:

$$SAR = \vec{E} \bullet \vec{J}_{conj}/(2\rho)$$

Afterwards the local SAR is averaged over a specific mass, usually 1g or 10g. As described in [IEEE P1528.4] the mass averaging is done by mapping the results to a structured hexahedral grid and afterwards the averaging scheme for FDTD per [IEEE P1528.4] is applied. The SAR calculation on the hexahedral grid is compliant with IEC 62704-1.

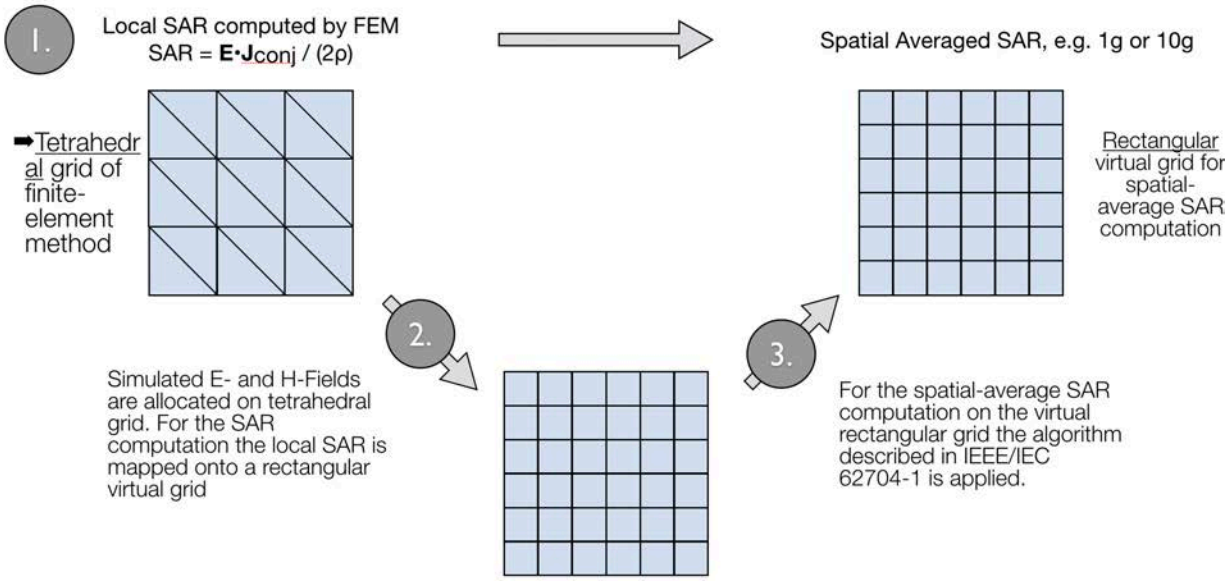

Figure 17: IEEE P1528.4 for SAR computation

4) Total Computational Uncertainty

Below is a table summarizing the budget of the uncertainty contributions of the numerical algorithm and of the rendering of the simulation setup. The table was filled using the IEC 62704-4, 2020. For the simulations, the extreme case where the phantom is placed directly in front of the puck is considered. As the phantom with particular reference dielectric parameters are used (as described in section 5); the corresponding phantom dielectric uncertainty is set to zero (section 7.2.6, IEC 62704-4, 2020).

Table 9: Budget of uncertainty contributions of the numerical algorithm (filled based on IEC 62704-4 2020).

a	b	d	e	g
Uncertainty component	Subclause	Probability distribution	Divisor f(d, h)	Uncertainty %
Mesh resolution	7.2.3	N	1	0.24
ABC	7.2.4	N	1	0.01
Power budget	7.2.5	N	1	0.08
Convergence	7.2.6	R	1,73	0.1
Phantom dielectrics	7.2.7	R	1,73	0
Combined standard uncertainty (k = 1)				0.27

Below is a table summarizing the budget of the uncertainty of the developed model of the DUT so far. The table was filled using the IEC 62704-4, 2020.

Table 10: Uncertainty of DUT Model

a	b	d	e	g
Uncertainty component	Subclause	Probability distribution	Divisor f(d, h)	Uncertainty %
Uncertainty of the DUT model (based on near field distribution)	7.2.2	N	1	0.27
Uncertainty of the measurement equipment and procedure	7.2.3	N	1	1.2
Combined standard uncertainty (k = 1)				1.23

The expanded (K=2) uncertainty result as per the IEC/IEEE 62704-1, 2017 and IEC/IEEE 62704-4, 2020 is listed in Table 11. The expanded standard uncertainty is 25.88, which is lower than the limit of 30.

Table 11: Expanded Standard Uncertainty

a	b	c	d	e	f	g	h
Uncertainty component	Sub clause	Tolerance %	Probability distribution	Divisor f(d,h)	c_i	Uncertainty %	v_i or v_{eff}
Uncertainty of the test setup with respect to simulation parameters	7.2		N	1	1	0.27	
Uncertainty of the developed numerical model of the test setup	7.3		N	1	1	1.2	
Combined standard uncertainty (k = 1)						1.23	
Expanded standard uncertainty (k = 2)						2.46	

Columns c, g and h shall be filled in based on the results of Table 5 and Table 6

NOTE 1 Column headings a to h are given for reference

NOTE 2 Abbreviation used in Table 11:

N – normal probability distribution

NOTE 3 The divisor is a function of the probability distribution and degrees of freedom (v_i and v_{eff})

NOTE 4 c_i is the sensitivity coefficient that is applied to convert the variability of the uncertainty component into a variability of SAR

The properties of the key materials of the DUT, as well as their tolerances, are listed in the following table.

Table 12: Material properties and tolerances

	Permittivity ±Tolerance	**Permeability ±Tolerance**	**Dielectric Loss tangent ±Tolerance**	**Magnetic Loss tangent ±Tolerance**	**Conductivity ±Tolerance**
Tx Ferrite	8596 +/-860	3336 +/-333.6	0.23 +/-0.023	0.12 +/-0.012	0
Rx Ferrite	12 +/-1.2	1347 +/-134.7	0.01 +/-0.001	0.22 +/-0.022	0
Tx Coil Copper	1	1	0	0	5.8e7
Rx Coil Copper	1	1	0	0	5.8e7

References:

1) IEC/IEEE 62704-4, 2020: “Determining the peak spatial-average specific absorption rate (SAR) in the human body from wireless communication devices, 30 MHz to 6 GHz – Part 4: General requirements for using the finite element method for SAR calculations.”
2) IEC/IEEE 62704-1, 2017: “Determining the peak spatial-average specific absorption rate (SAR) in the human body from wireless communications devices, 30 MHz to 6 GHz - Part 1: General requirements for using the finite difference time-domain (FDTD) method for SAR calculations.”
3) The electrical conductivity of human cerebrospinal fluid at body temperature, S.B. Baumann ; D.R. Wozny ; S.K. Kelly ; F.M. Meno, IEEE Transactions on Biomedical Engineering (Volume: 44 , Issue: 3 , March 1997)
4) https://itis.swiss/virtual-population/tissue-properties/database/thermal-conductivity/
5) C.Gabriel, S.Gabriel and E.Corthout: The dielectric properties of biological tissues: I. Literature survey, Phys. Med. Biol. 41 (1996), 2231-2249.
6) S.Gabriel, R.W.Lau and C.Gabriel: The dielectric properties of biological tissues: II. Measurements in the frequency range 10 Hz to 20 GHz, Phys. Med. Biol. 41 (1996), 2251-2269.
7) S.Gabriel, R.W.Lau and C.Gabriel: The dielectric properties of biological tissues: III. Parametric models for the dielectric spectrum of tissues, Phys. Med. Biol. 41 (1996), 2271-2293.
8) X. L. Chen et al., "Human Exposure to Close-Range Resonant Wireless Power Transfer Systems as a Function of Design Parameters," in IEEE Transactions on Electromagnetic Compatibility, vol. 56, no. 5, pp. 1027-1034, Oct. 2014.
9) http://hyperphysics.phy-astr.gsu.edu/hbase/magnetic/toroid.html